Journal of The Electrochemical Society, 2020 **167** 022509

Influence of Furil Dioxime on Cobalt Electrochemical Nucleation and Growth

Y. Hu,[1,*] T. Lyons,[1] and Q. Huang[1,2,*,z]

[1]*Department of Chemical and Biological Engineering, University of Alabama, Tuscaloosa, 35487 Alabama, United States of America*
[2]*Alabama Water Institute, University of Alabama, Tuscaloosa, 35487 Alabama, United States of America*

The nucleation and growth of cobalt (Co) on blanket Si with extremely thin Co seed was studied in the presence of furil dioxime (FD). Cyclic voltammetry (CV), chronoamperometry, and galvanostatic nucleation studies were conducted to understand the effects of FD on Co nucleation process. A potential dependent suppression effect was observed at low potential with a breakdown of the suppression at high potential, resulting in a hysteresis in CV. The potentiostatic current transient experiments showed that side reactions and adsorption process both greatly affected Co nucleation. A well-established model, which deconvolutes the individual contributions to the total current transient, was applied to fit the experimental curves. Progressive and instantaneous Co nucleation were observed across different FD concentrations and applied potentials. Galvanostatic studies further proved the suppression effect of FD and the effects on film morphology were studied at different conditions.
 [DOI: 10.1149/1945-7111/ab69fb]

Manuscript submitted November 11, 2019; revised manuscript received December 28, 2019. Published January 23, 2020.

Supplementary material for this article is available online

As the semiconductor integrated circuits evolve into 7 nm technology and beyond,[1] the concerns about copper (Cu) interconnects increase. The resistance of the finest copper lines at the ground rule metal level in back-end-of-line interconnects no longer linearly scales with dimension.[2,3] Instead, the resistivity starts to increase exponentially because the electron scattering at grain boundaries and interfaces rapidly dominates the overall resistance.[4,5] High resistivity not only consumes more energy and demands faster heat dissipation, but also results in a greater RC delay in the circuit.[6] This cancels out the performance gain resulted from scaling and front-end device innovations. To address the resistivity issue, alternative metals like cobalt (Co) is thought as a promising material due to its higher melting point and shorter mean free path. The former relates to a lower risk of electromigration, whilst the latter decreases the contribution from electron scattering at grain boundaries and interfaces.

Copper bottom-up filling process has been well established.[7–15] Varieties of additives known as accelerator, suppressor and leveler were systematically classified.[16] Different influencing factors such as electrolyte,[14,17,18] applied potential[19] were thoroughly investigated. Curvature Enhanced Accelerator Coverage (CEAC) mechanism[11] was proposed not only to explain how additives affect the Cu filling process but also to enable the filling of other metals such as gold,[20–22] silver[23–25] and nickel.[26] However, studies on Co electro-filling process has been rarely reported until recently. S-shaped negative differential resistance (S-NDR) mechanism was introduced to explain the superconformal Co electrodeposition in high aspect ratio through silicon vias (TSV).[27] Recently, defect-free filling of Co has been achieved using proprietary additives. The additives play an important role in such processes creating differential plating rates between the feature bottom and field regions because of a current efficiency difference[28,29] or a hydrogen-induced deactivation of additives.[30] Different functional groups in organic additives were found to influence the deposition kinetics.[31–34] In our previous study,[35–37] additives with a conjugated pair of oxime groups such as dimethylglyoxime (DMG) and cyclohexane dioxime (CHD) displayed strong suppression effects on Co deposition and a suppression breakdown occurred upon the reduction of adsorbed Co^{2+}-dioxime chelates.

Previous study[35] on the Co nucleation with DMG and CHD showed an interesting "two-peak" phenomenon, where two different nucleation peaks were observed in presence of these dioximes due to a hypothesized two-step reduction mechanism. This paper presents a study of the effects of furil dioxime (FD), a molecule with not only the pair of conjugated oxime groups but also additional multiple conjugated C=C bonds in the furil groups, on Co nucleation process. Cyclic voltammetry, galvanostatic deposition, potentiostatic nucleation, as well as numerical curve fitting were carried out not only to understand the effects of FD on Co deposition and nucleation but also to deconvolute the current contributions from nucleation and other competing reactions. A descriptive model of the nucleation process was provided.

Experimental

A traditional three-compartment electrochemical cell was used for the experimental studies, where the catholyte and anolyte were separated by a glass frit. A saturated calomel electrode (SCE, 0.24 V vs NHE) was used as the reference electrode, and all potentials were referred to this SCE in this report. The reference electrode compartment was connected to the catholyte through a capillary. The counter electrode was a Co foil with a surface area much larger than the cathode. Si coupons cleaved from a 12-inch blanket wafer with Co (5 nm, CVD) on TiN (5 nm, CVD) were used as cathodes. A circular deposition area of 0.385 cm^2 was defined with plating tape. The thin Co seed was used to mimic the substrates used in industry and to provide enough conductivity for the electrodeposition studies. However, this seed layer was not expected to be continuous and Co electrodeposition behavior was strongly influenced by the underneath TiN layer. The wafers were shipped and stored in ultrahigh pure nitrogen ambient until immediately before the experiments to minimize the surface oxidation. The substrates were used as received without further treatment.

The Co makeup solution for CV studies was the same as our previous study,[35] containing 0.3 M $CoSO_4 \cdot 7H_2O$, 0.4 M H_3BO_3, and 0.1 g l^{-1} sodium dodecyl sulfate (SDS). The pH was adjusted to 4.0 with H_2SO_4 and NaOH. Concentrated furil dixoime (FD) solutions (2800 ppm) were prepared by dissolving the corresponding chemical powder in a 1:1 water ethanol mixture. Calculated amounts of the concentrate were then added into the Co makeup solution up to various final concentrations. Another diluted version of Co makeup solution containing 0.01 M $CoSO_4 \cdot 7H_2O$, 0.1 M Na_2SO_4,

*Electrochemical Society Member.
[z]E-mail: qhuang@eng.ua.edu

0.4 M H_3BO_3, and 0.1 g l^{-1} SDS with a pH of 4.0 was used to study the Co nucleation process. All salts and organic additives were at least ACS grade and used as received. Deionized (DI) water with a resistivity of 18.2 MOhm-cm was used in all studies.

Co nucleation was studied using electrochemical techniques (cyclic voltammetry, chronoamperometry and galvanostatic deposition). An Autolab 302 N potentiostat was used for all electrochemical studies. The chronoamperometry curves acquired during nucleation were analyzed and fit using the Polynomial Fit option in Origin™ 8.0. Surface morphology of the deposited Co nuclei was examined with a JEOL 7000 field emission scanning electron microscope (SEM) operated at 30 kV.

Results and Discussion

The impact of FD on Co electrodeposition was first studied with cyclic voltammetry (CV) in the Co makeup electrolytes. Figure 1 shows the CV results at different concentrations of FD. The current density started to decrease at around −0.70 V in the absence of FD, but the drop of current density at the beginning did not result from Co deposition. The chronoamperometry studies on the nucleation (Fig. 2a) showed that the Co deposition started between −0.80 V and −0.85 V when no additive was added. Therefore, the initial decrease of the current density was considered as hydrogen evolution reaction. The addition of 10 ppm FD caused a minor suppression of Co deposition, where Co deposition was seen at a potential of −0.82 V. A small hysteresis was observed, where the current density was slightly higher on the reverse (anodic) sweep at around −0.82 V. Increasing FD concentration to 100 ppm further suppressed the Co deposition till up to −1.1 V. The deposition current density increased rapidly from −0.5 mA cm^{-2} to −10 mA cm^{-2} when the potential scanned from −1.10 V to −1.20 V. The Co deposition potential was further delayed to −1.23 V and −1.30 V with the addition of 300 ppm and 500 ppm FD, respectively. In our previous study,[37] the Co deposition potential was respectively delayed to −1.0 V and −1.05 V with the addition of 300 ppm DMG and CHD, which indicated that the suppression effect of FD was stronger than these two different dioxime additives. A pronounced hysteresis was observed for all the three cases with over 100 ppm FD. While a stronger suppression was observed in the forward scan when the FD concentration increased from 100 to 300 and 500 ppm, the deposition current extended to a same potential of about −0.85 V on the reverse scan for all three cases. The surface adsorption of Co^{2+}-dioxime complex and its reduction was proposed as the mechanism for the suppression and consumption-based suppression breakdown. The higher stability constant between Co^{2+} and FD than DMG and CHD is consistent with the stronger suppression reported here.

Figure 2 depicts families of potentiostatic current density transients obtained during cobalt nucleation and growth on blanket wafer at different overpotentials. Figure 2a shows the Co nucleation results without FD. Co nucleation did not happen at −0.80 V because the threshold overpotential for deposition was not reached, as discussed in the CV curves (Fig. 1). It was clear that Co nucleation occurred at −0.85, −0.90, −0.95, −1.0, and −1.1 V. An initial sharp current decay was observed, which corresponded to the double layer charging and surface adsorption. The current decay is potential dependent and does not follow the $t^{-1/2}$ relation described by the Cottrell's equation for mass transport limited decay. Instead, it follows an exponential decay, a characteristic of capacitive behavior. This rapid decay was followed by a current rise due to an increase in the deposition area associated with nucleus formation on the substrate. After reaching a maximum, the current density gradually decreased again upon the development of a mass transport limited process. All cases at these five potentials followed the same trend. An ideal mass transport limited current decay during potentiostatic deposition can be described with the so-called Cottrell equation.[38] However, the currents in this study did not decay to 0 but

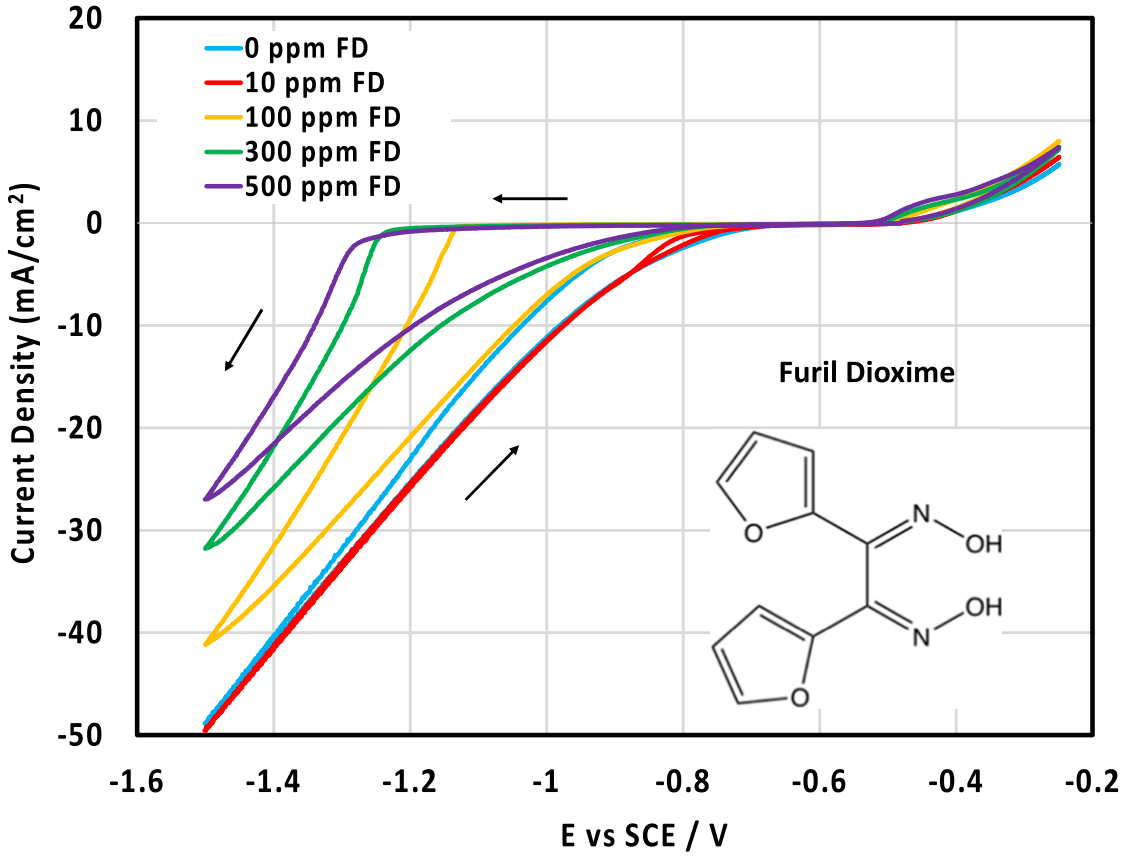

Figure 1. Cyclic voltammetry of Co electrodeposition at different FD concentrations.

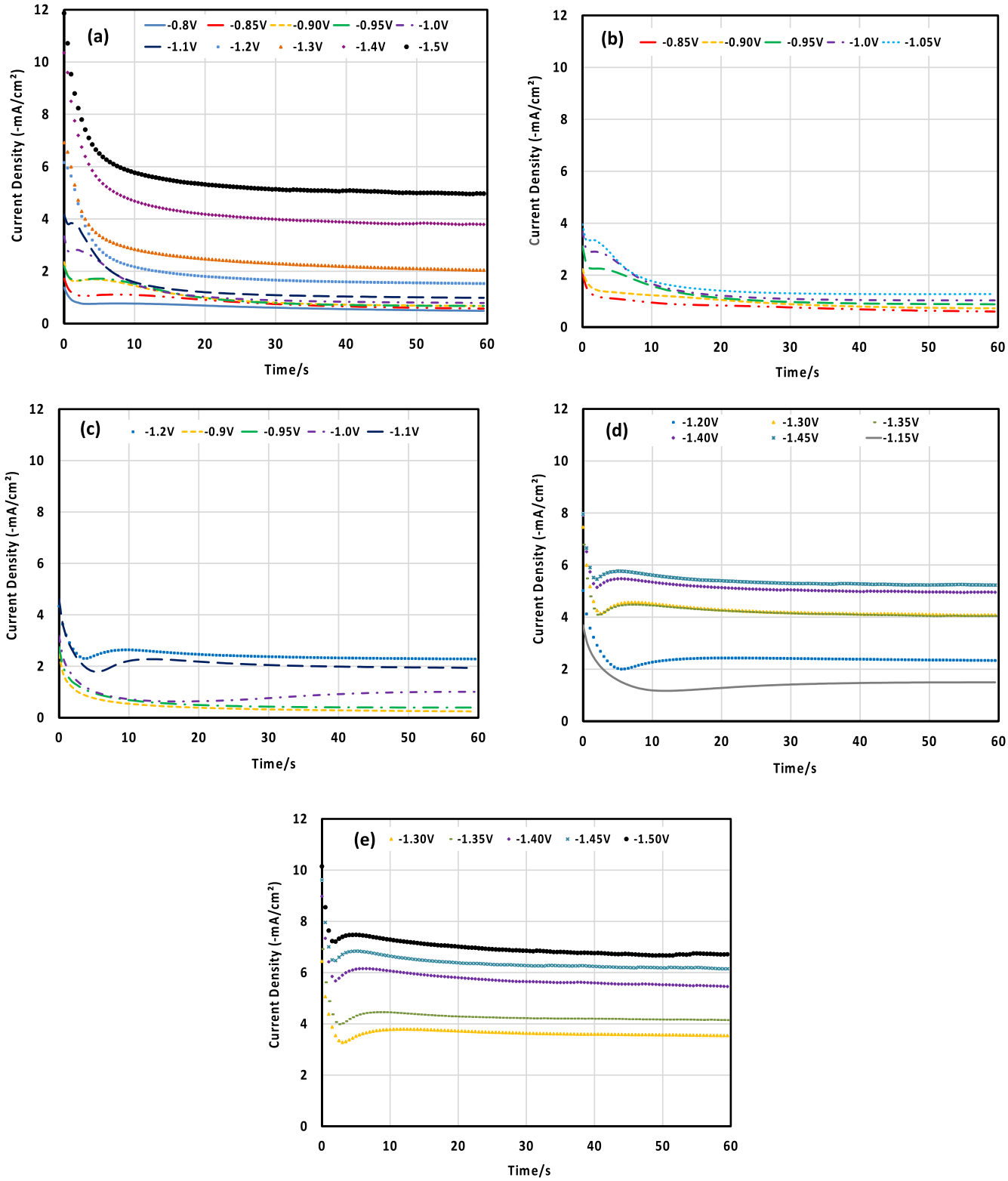

Figure 2. Current transients for cobalt deposition on thin Co seed blanket wafer at different potentials in 0.01 M Co solutions with (a) 0-ppm (b) 10-ppm (c) 100-ppm (d) 300-ppm (e) 500-ppm FD.

stayed at a constant of around $-1.5\ \text{mA cm}^{-2}$. This steady state current density was believed to relate to the side reactions such as the two below.

$$2H^+ + 2e \rightarrow H_2 \quad [1]$$

$$2H_2O + 2e \rightarrow H_2 + 2OH^- \quad [2]$$

Since cobalt deposition occurs at a comparably negative potential, the hydrogen evolution reaction inevitably occurs. However, the nucleation current peaks were still evident in the curves because they

emerged at a time where the capacitance currents had significantly decayed and the side reaction currents were low. On the other hand, the proton reduction (Eq. 1) and water reduction (Eq. 2) dominated the total current when the overpotential was more negative than −1.1 V, resulting in the rapid increase of steady state current density as the potential became more negative. For example, while this current density was only around $-1.5\ \text{mA cm}^{-2}$ at −1.1 V, it reached $-5.5\ \text{mA cm}^{-2}$ at −1.5 V as the water reduction became more pronounced at such a negative potential.

Figure 2b shows the same current transients during Co nucleation with 10 ppm FD. Co nucleation did not take place at −0.85 or −0.90 V but −0.95 V due to the suppression effect of FD. It seemed to contradict with the CV results, where the Co deposition occurred at around −0.82 V with the addition of 10 ppm FD. However, it is worth noting that two different concentrations of Co, 0.3 M and 0.01 M, were separately used for CV and nucleation studies. The small amount of FD was not enough to completely deplete free Co^{2+} in either solution and the deposition behaviors were expected to be similar as there were plenty of Co^{2+} near the electrode. Nevertheless, the suppression effect would be more evident when a low overall concentration of Co^{2+} is used, which explains why more negative potential was required to initiate the Co deposition in the nucleation study. Figure 2c describes the same studies with 100 ppm FD, where a stronger suppression effect was observed. Co nucleation started at a more negative threshold potential of −1.0 V. As shown in Figs. 2d and 2e, increasing the FD concentration to 300 ppm or 500 ppm further suppressed the Co nucleation. In addition, the higher FD concentration also resulted in a significant increase in the steady state current density. For instance, the magnitude of steady state current density at −1.4 V was $4\ \text{mA cm}^{-2}$ in the FD-free electrolyte, while it increased to $5.5\ \text{mA cm}^{-2}$ with 500 ppm FD. Co^{2+}-dioxime complex is known to act as an electrocatalyst for hydrogen evolution reactions.[39,40] While the detailed chemical mechanism and the exact speciation of the catalyst are still under debate,[41–43] the Co cation chelated with multiple N-atoms and the conjugated C=C and C=N double bonds in the organic molecule is expected to be involved. It is believed that such a complex accelerated the production of hydrogen on the surface of newly deposited Co,[44] resulting in the increase of steady state current density.

The current transient curves during potentiostatic nucleation of Co with a simpler dioxime molecule, dimethylglyoxime or DMG, were reported previously to show two current peaks, resulting from a two-step reduction reaction. The first peak corresponded to the reduction of Co^{2+}-dioxime chelate adsorbed on the surface, and the reduction of free Co^{2+} cations was responsible for the second peak. While such double peak curves were not observed in this study, it is believed that the two-step deposition mechanism remains the same in presence of FD. The Co^{2+} reduction reaction is related to the nucleation peak in the FD-free electrolyte. As the potential decreases to below −1.2 V, the proton and water reduction reactions gradually become more pronounced and dominant. When 10 ppm FD is added into the solution, only a small amount of Co-FD complexes are formed and the majority of Co^{2+} cations remain free in the solution. The nucleation curves are similar to the FD-free cases.

In the presence of 100 ppm or more FD, the complexed Co^{2+}-FD chelates are still of a small fraction of the total Co^{2+}. The complex adsorbs on an active site on the electrode resulting in strong suppression. Subsequently, the Co^{2+} chelate reduction reaction occurs upon the application of a voltage more negative than the threshold value and the chelate is quickly reduced. Co nuclei are formed on the electrode and the organic fragments of dioxime are desorbed from electrode or get incorporated into the film during this process. Immediately afterwards, the reduction of free Co^{2+} cation starts. These two Co reduction processes both lead to nuclei formed on the electrode and an increase of the overall reactive area. They would have also resulted in two distinct nucleation peaks in an ideal situation. However, the strong suppression effect of FD requires a highly negative potential to overcome, at which the reduction of free Co^{2+} becomes extremely rapid. Therefore, the Cottrell decay is expected to occur immediately upon the reduction of Co-FD complex, convoluting the two nucleation steps. In addition, and probably more importantly, the surface area of nuclei increases rapidly and the hydrogen evolution reaction on the newly emerged surface becomes so overwhelming at these potentials that they not only amplify the nucleation current, i.e. the increase of nucleus surface area, but also further mask and convolute the two nucleation current peaks. It is believed that this "amplification effect" is the main reason for the single nucleation peak observed across all high FD concentrations.

Metal deposition on foreign substrates including thin seeded substrate typically follows the so-called Volmer-Weber three-dimensional nucleation with diffusion-controlled growth of nuclei.[45,46] Such behaviors have been well studied and mathematically described.[47,48] For the two extreme cases, the ideal progressive and instantaneous nucleation processes, the current transient responses for a potential step on a stagnant electrode are described by the following equations:

Instantaneous nucleation

$$i(t) = \frac{zFD^{1/2}c}{\pi^{1/2}t^{1/2}}[1 - \exp(-N\pi kDt)] \quad [3]$$

Progressive nucleation

$$i(t) = \frac{zFD^{1/2}c}{\pi^{1/2}t^{1/2}}\left[1 - \exp\left(-\frac{1}{2}AN_{\infty}\pi k'Dt^2\right)\right] \quad [4]$$

where z is the number of electrons transferred during Co nucleation, F is the Faraday constant, D is the diffusion coefficient of Co^{2+}, c is the bulk concentration of Co^{2+}, t is the time, A is the steady state nucleation rate constant per site, N is the number of nuclei, N_{∞} is the maximum number of nuclei obtainable, k and k' are dimensionless constants, where $k = (8\pi cM/\rho)^{1/2}$ and $k' = 4/3(8\pi cM/\rho)^{1/2}$. A simplified form can be obtained by nondimensionalizing the current and time with the values at the current peak, i_{max} and t_{max}.

Instantaneous nucleation

$$\frac{i(t)}{i_{max}} = \left\{\frac{1.9542}{(t/t_{max})}\left[1 - \exp\left(-1.2564\frac{t}{t_{max}}\right)\right]^2\right\}^{1/2} \quad [5]$$

Progressive nucleation

$$\frac{i(t)}{i_{max}} = \left\{\frac{1.2254}{(t/t_{max})}\left[1 - \exp\left(-2.3367\left(\frac{t}{t_{max}}\right)^2\right)\right]^2\right\}^{1/2} \quad [6]$$

The nucleation current transients in Fig. 2 where a current peak was observed were normalized with the current peaks and are presented together with the ideal instantaneous and progressive nucleation cases in Fig. S-1 in Supplemental Material (available online at stacks.iop.org/JES/167/022509/mmedia). Since the total current is the result of different processes, and cannot be treated as Co nucleation alone, the deviation of experimental data from ideal model is observed in all cases studied. Efforts are therefore aimed to deconvolute the total current density $i_{total}(t)$ following a method proposed by Manuel Palomar-Pardavé et al., where the side reactions and adsorption process were taken into consideration.[49–53] Hydrogen produced in the side reactions are assumed to dissolve into the electrolyte or detach from the electrode immediately upon formation. Such detachment is possible as SDS is used in the electrolytes as a surfactant. However, the bubbles have to be extremely small so that the agitation effect of such detachments can be negligible during the nucleation process. While the experimental quantification of the effects of hydrogen bubble is extremely challenging and worth future exploration, the assumption here that the hydrogen produced from the side reaction does not block the electrode surface simplifies

the decomposition of the total current. The contributions from diffusion controlled 3-dimensional nucleation and growth, $i_{3D}(t)$, as well as other processes including the capacitive adsorption, $i_{ad}(t)$, and side reactions on the surface of Co nuclei, $i_{side}(t)$, can be described with the following equations.

$$i_{total}(t) = i_{ad}(t) + i_{3D}(t) + i_{side}(t) \quad [7]$$

$$i_{ad}(t) = i_{ad0} \exp(-t/\tau_{ad}) \quad [8]$$

$$i_{3D}(t) = C_{cottrell} t^{-\frac{1}{2}} \frac{\phi}{\varphi} \theta(t) \quad [9]$$

$$i_{side}(t) = C_{side} \frac{\phi}{\varphi} \theta(t) \quad [10]$$

In these equations, i_{ad0}, τ_{ad}, $C_{cottrell}$, and C_{side} are time independent constants characterizing various processes. While some of them can be further described with physical parameters, some only depend on empirical parameters. Nevertheless, these time independent constants can be potential dependent and therefore can be obtained by fitting the experimental current transients at different potentials. On the other hand, θ is the actual fraction of area covered by diffusion zone, ϕ is the "retardation" of the current by slow nucleation,[54] and φ is the "retardation" of the growth of the extended coverage.[54] The ratio between ϕ and φ represents a correction factor to covert the projected 2D extended surface coverage, θ, into the actual 3D surface area of nuclei. All these three are time dependent parameters and have to be further described as functions of time with time independent coefficients, as shown in following equations.

$$\theta(t) = 1 - \exp[-C_{coverage} \cdot t \cdot \varphi(t)] \quad [11]$$

$$\varphi(t) = 1 - \frac{1 - \exp(-At)}{At} \quad [12]$$

$$\phi(t) = 1 - \frac{\exp(-At)}{(At)^{\frac{1}{2}}} \int_0^{(At)^{\frac{1}{2}}} \exp(\lambda^2) d\lambda \cong 1 - \frac{0.0513 + 0.479 \cdot (A \cdot t)^{\frac{1}{2}}}{[1 - 1.207 \cdot (A \cdot t)^{\frac{1}{2}} + 1.186 \cdot (A \cdot t)] \cdot (A \cdot t)^{\frac{1}{2}}} \quad [13]$$

The numerical values of A, the steady state nucleation rate constant per site, and other parameters such as $C_{coverage}$ are both independent of time and could be obtained by fitting the current transient curves. Thus, the model described by Eq. 7 can be used to fit the experimental current transients and allow the deconvolution of each different contribution during the Co nucleation. Overall, there are six fit parameters across Eqs. 7–13 i_{ad0}, τ_{ad}, $C_{cottrell}$, C_{side}, $C_{coverage}$, and A, all of which are all potential or additive concentration dependent.

Figure 3 shows some examples of experimental current transients at different potentials and FD concentrations and the current breakdown obtained with non-linear fitting of the experimental data. The fit parameters are listed in Table I. It can be seen that i_{ad0} and τ_{ad} are strongly dependent on the applied potential, but the effect of additive concentration is minimal. This is consistent with the capacitive charging or adsorption behavior of the double layer. On the other hand, the two parameters describing surface coverage and cobalt nucleation rate, $C_{coverage}$ and A, are strongly dependent on the additive concentration. The time independent prefixed ratio constants for the time dependent current transients of Co deposition and hydrogen evolution reaction, $C_{cottrell}$ and C_{side}, respectively, are mainly dependent on the diffusion coefficients of cation species and are both relatively independent of additive concertation. Additional curve fittings were included in Fig. S-2 in the Supplemental Materials. Figure 3a shows the Co nucleation at −1.0 V without FD. It is evident that the experimental current transient can be well described with the theoretical equations with the fit parameters. The adsorption process started immediately when the potential was applied and this capacitive current decayed to a negligible value after 23 s. The Co nucleation and side reaction also started simultaneously upon the application of potential, gradually increasing with time. As depicted in Eqs. 9 and 10, the descriptive model here assumed that both the Co nucleus growth and hydrogen evolution reactions only occurred on the Co nuclei. Therefore, both currents increased simultaneously along with the surface coverage, θ, corrected with the ratio between the 3-dimensional surface area and the 2-dimensional coverage projected on the electrode surface, ϕ/φ. As the deposition continued, the Co nucleation current density, i_{3D}, gradually became governed by the Cottrell decay, as described by the $t^{-\frac{1}{2}}$ term in Eq. 9, resulting in a current peak. On the other hand, the side reaction remained at a constant after 10 s because the surface coverage, θ, approaches 1, and the water molecules were in excessive amount. Figure 3b shows the Co nucleation at −1.0 V with 10 ppm FD. The steady state current density for side reactions slightly increased. This was believed to relate to the catalytic effect of $Co(FD)_2$ for hydrogen evolution reaction. Due to the presence of conjugated C=C bonds and the C=N bonds, the catalytic effect was expected to be even stronger than those without conjugated C=C bonds such as DMG and CHD.[55] On the other hand, the current density for Co nucleation remained unchanged or slightly decreased from the FD-free case because of the suppression effect of FD on Co deposition. Figures 3c–3d show the decomposed current densities during Co nucleation with two FD concentrations at −1.2 V, where a similar trend was observed in both cases. Namely, as the FD increased from 100 ppm to 300 ppm, the current density of side reaction increased whilst Co nucleation current slightly dropped. The enhancement of side reaction was insignificant in this case, where the catalytic effect of $Co(FD)_2$ had been saturated at this applied potential. Figure 3e shows the Co nucleation with 500 ppm FD at −1.4 V, where an overwhelming water reduction was clearly observed.

The numerical fitting and deconvolution of the chronoamperometry curves not only allow to break down the contributions of different electrochemical reactions on the surface, but also enable further analysis of the nucleation behavior. Figure 4 shows the Co nucleation current transients obtained from the numerical fitting shown in Fig. 3, normalized with the current peak. The ideal progressive and instantaneous nucleation processes were also included for comparison. It was interesting to find that almost all the Co cases studied followed a progressive nucleation process. The two exceptions were the cases with 100 ppm and 300 ppm FD at −1.2 V, where a more instantaneous nucleation character was observed. Progressive nucleation has been widely observed in electrochemical deposition of metal on non-metallic substrates, such as Si and glassy carbon.[49,56,57] The TiN substrate used in this study was expected to have a thin layer of oxide, resulting in a non-metallic surface.

Galvanostatic deposition at different current densities of −2, −4 and −10 mA cm^{-2} were carried out to microscopically examine the effects of FD on Co nucleation. A constant charge density of −15.58 mC cm^{-2} was used. The deposition time needed for this charge density varied up to 7.79 s, corresponding to a small portion at the beginning of current transients shown in Fig. 2. Figure 5 shows the top down SEM images of deposits. Needle-shaped Co nuclei were deposited from the additive free electrolyte. Nuclei with various sizes were observed, consistent with the progressive nucleation behavior determined on the current transients in Fig. 4. Deposition at −4 mA cm^{-2} resulted in the highest density and the largest size of Co nuclei, which may correspond to the highest current efficiency. Little suppression effect was observed at a low concentration of 10 ppm FD on Co deposition, consistent with the results from electrochemical studies. The nucleation density significantly decreased as the FD concentration increased to 100 ppm at −4 mA cm^{-2}, and a smaller size of cobalt nuclei was observed at −2 and −10 mA cm^{-2}. A change in nucleus shape and decrease in

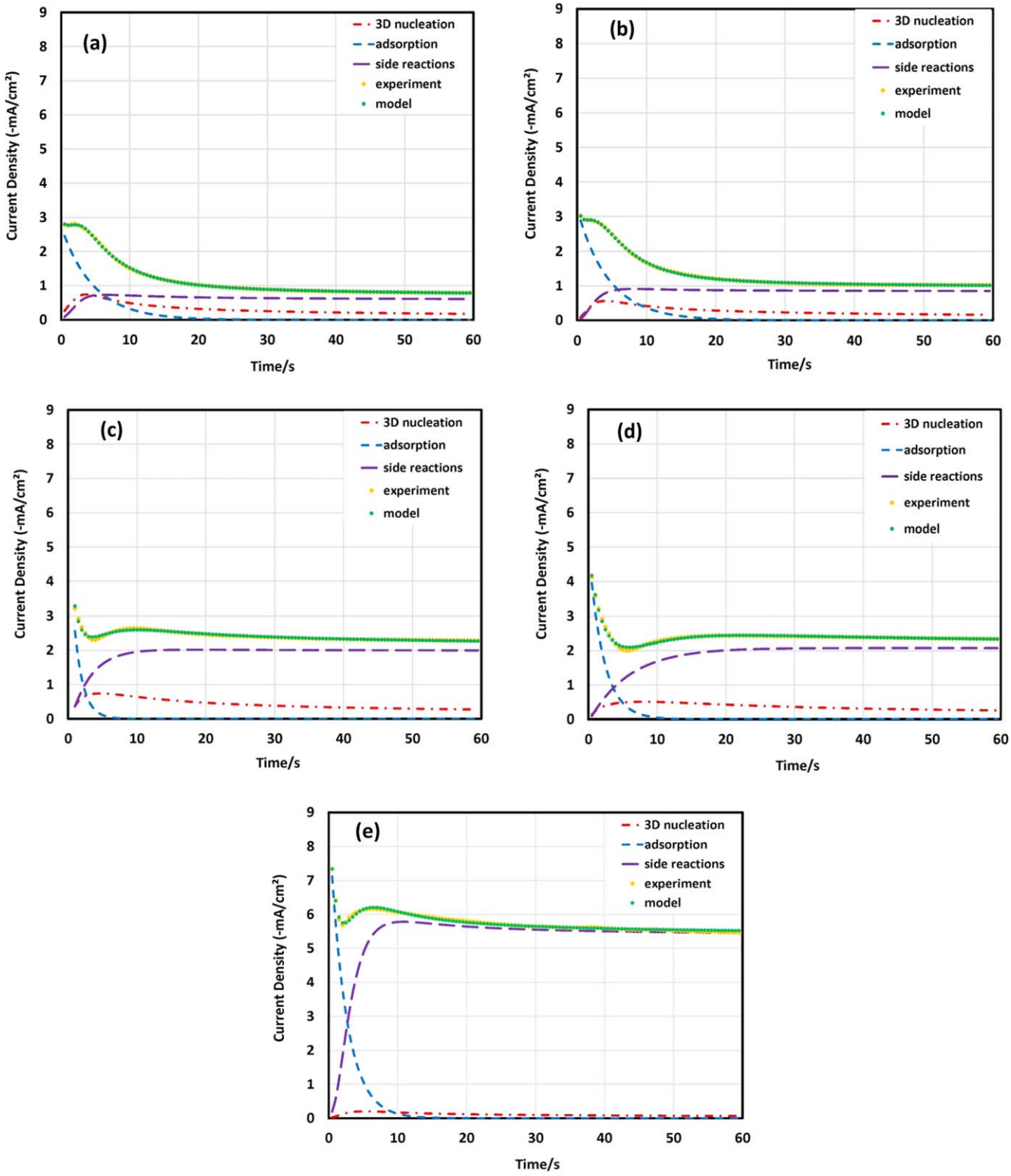

Figure 3. Individual contributions to the experimental Co nucleation current transients due to the adsorption process, Co nucleation process and side reactions at (a) 0-ppm, −1.0 V (b) 10-ppm, −1.0 V (c) 100-ppm, −1.2 V (d) 300-ppm, −1.2 V (e) 500-ppm, −1.4 V.

nucleus number were observed upon the further addition of FD up to 300 ppm. Spherical Co nuclei in addition to the needle-shaped ones were observed across all current densities studied. Specifically, the number of Co nuclei drastically decreased and only two spherical Co nuclei were observed at -4 mA cm^{-2}. The addition of 500 ppm FD resulted in little difference compared with the 300 ppm FD case. One interesting finding was that there were more needle-shaped Co nuclei at -2 mA cm^{-2} with 500 ppm FD. However, more spherical Co nuclei were formed at -10 mA cm^{-2}.

Galvanostatic deposition with extended deposition time was conducted to further study the morphology of Co film, i.e., the growth of Co grains. In this set of experiments, Co deposition was

Table I. The fit parameters used to decompose the experimental current transients in Fig. 3.

Potential (V)	FD concentration	i_{ad0} (mA cm^{-2})	$1/\tau_{ad}$ (s^{-1})	$C_{cottrell}$ (mA cm^{-2}s$^{-1/2}$)	C_{side} (mA cm^{-2})	$C_{coverage}$ (s^{-1})	A (s^{-1})
−1.0V	0-ppm	2.7300	0.21377	1.27475	0.58594	2.29474	0.20237
−1.0V	10-ppm	3.2155	0.21853	1.20417	0.83724	0.61919	0.55943
−1.2V	100-ppm	5.6418	0.78972	2.05634	1.98398	0.32457	1.49307
−1.2V	300-ppm	4.9966	0.46934	1.95293	2.06556	0.16650	2.65070
−1.4V	500-ppm	8.7783	0.41869	0.49378	5.35393	0.46385	0.46211

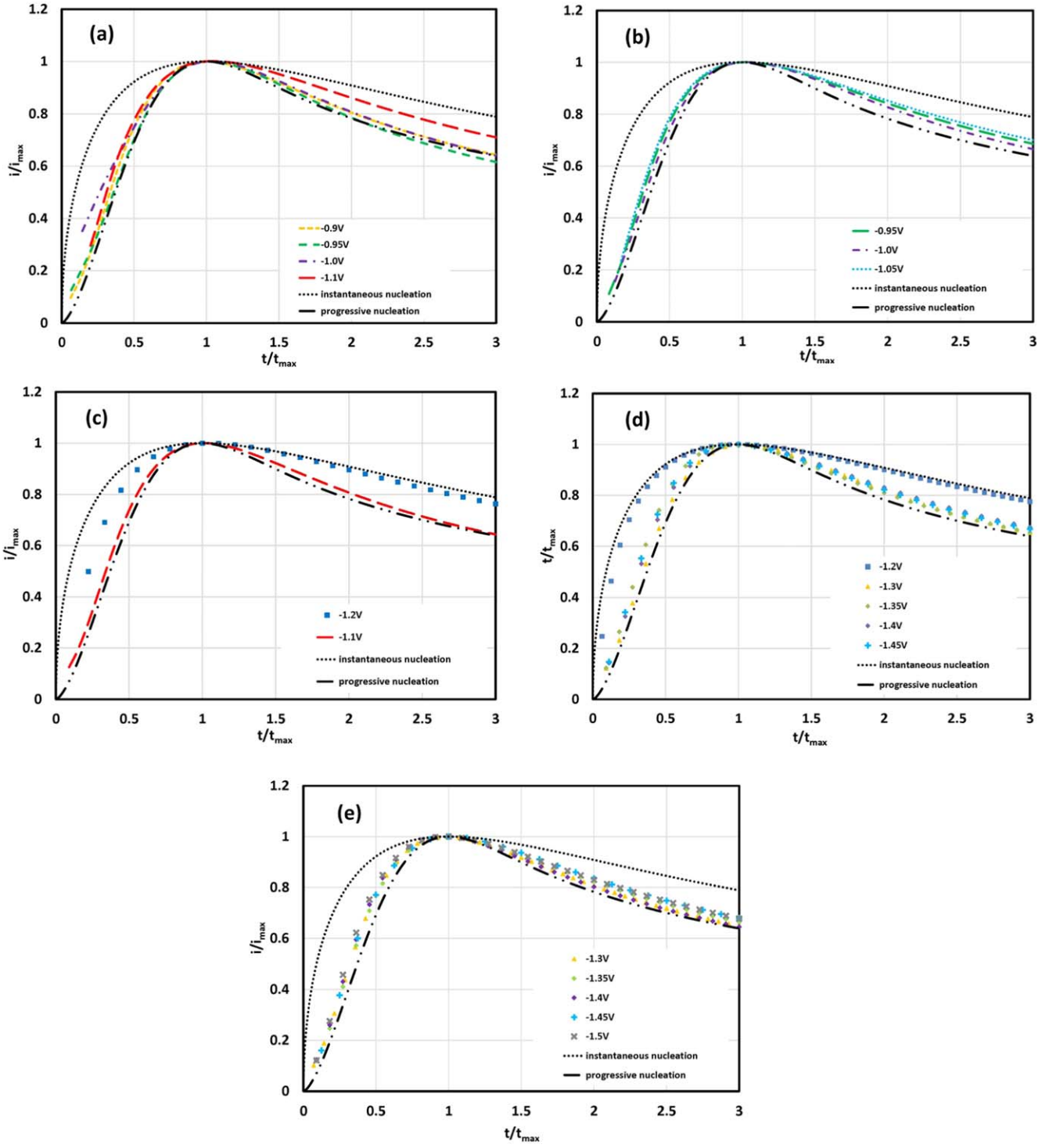

Figure 4. Comparison of experimental normalized Co nucleation current transients with instantaneous and progressive nucleation model at (a) 0-ppm (b) 10-ppm (c) 100-ppm (d) 300-ppm (e) 500-ppm FD.

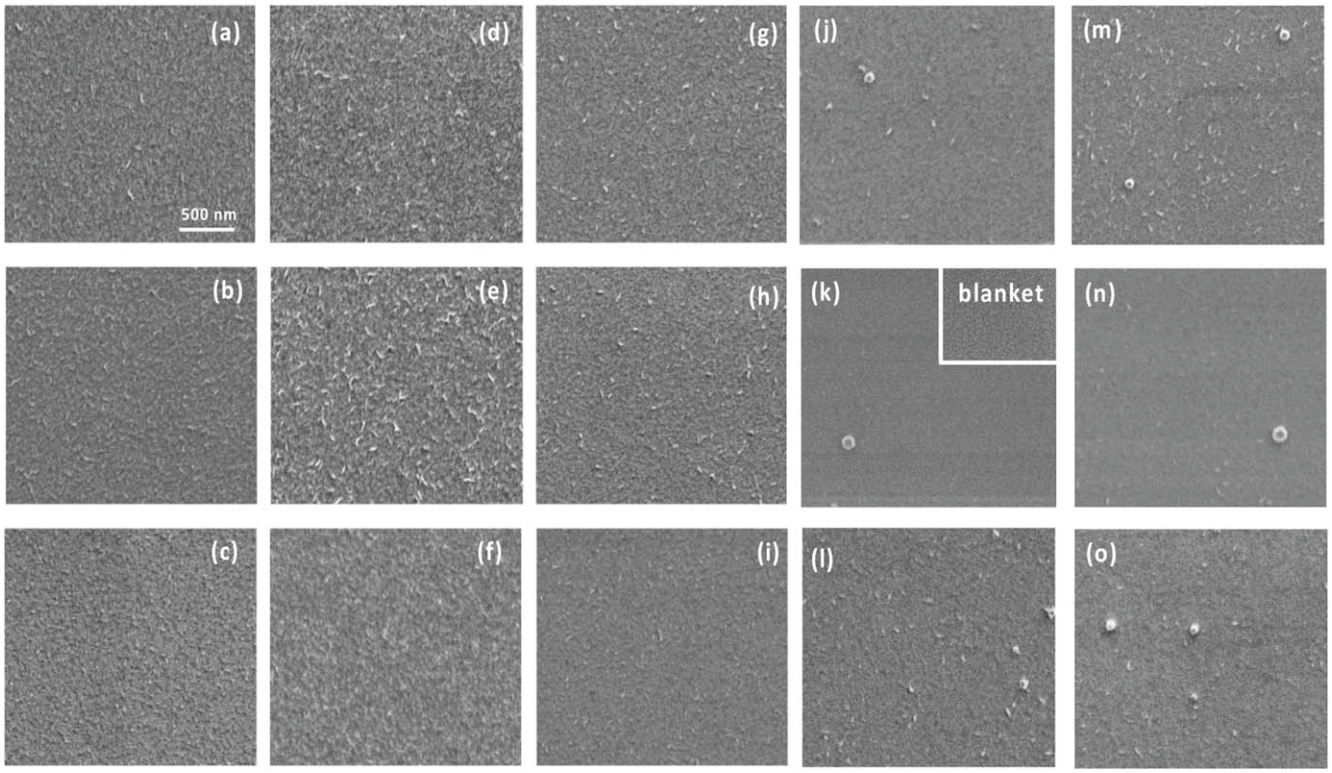

Figure 5. SEM images of cobalt nuclei deposited thin Co seed blanket wafer from solution containing 0.01 M Co with (a-c) 0, (d-f) 10, (g-i) 100, (j-l) 300, (m-o) 500 ppm FD at (a,d,g,j,m)—2, (b,e,h,k,n)—4, and (c,f,I,l,o)—10 mA cm^{-2}. The total deposition charge was—15.58 mC cm^{-2}. The blanket substrate was shown in (k).

respectively conducted at -2 and -4 mA cm^{-2} for 500 s with the addition of 100 ppm FD in 0.01 M Co solution. Figure 6 shows the top down SEM images of the deposits. The Co nuclei grew much bigger with the grains of 100 nm. However, needle-shaped ridges of Co grains were still evident regardless of the deposition current used in the study. Also, fewer Co nuclei with needle-shaped ridge were observed at -4 mA cm^{-2} than -2 mA cm^{-2}.

Surfactants are known to alter the crystal growth behavior by selectively adsorbing and blocking certain crystalline facets.[58–60] The crystals formed therein grow preferably in the unblocked facets and result in planes or ridges in different directions. A lower current is expected to allow the nuclei or grains to grow at a more equilibrium state, where a strong influence by the surfactant adsorbates would be expected. On the other hand, a higher current density may force the crystals to grow even at the facets with surfactant adsorbate, resulting in less ridges and more randomly shaped grains, as observed in Fig. 6b.

Conclusions

The effect of a dioxime molecule with conjugated C=C bonds, furil dioxime, on Co electrodeposition was studied. Suppression effect on Co deposition by FD was observed in CV as well as chronoamperometry nucleation studies. While the threshold potential for nucleation decreased upon the increase of FD concentration, the reduction reactions of proton and water were much facilitated at the same time. The total current transients during potentiostatic nucleation were deconvoluted into contributions from the capacitive charging, 3-D Co nucleation and growth, and the surface area dependent side reaction. Not only the $Co(FD)_2$ complex was

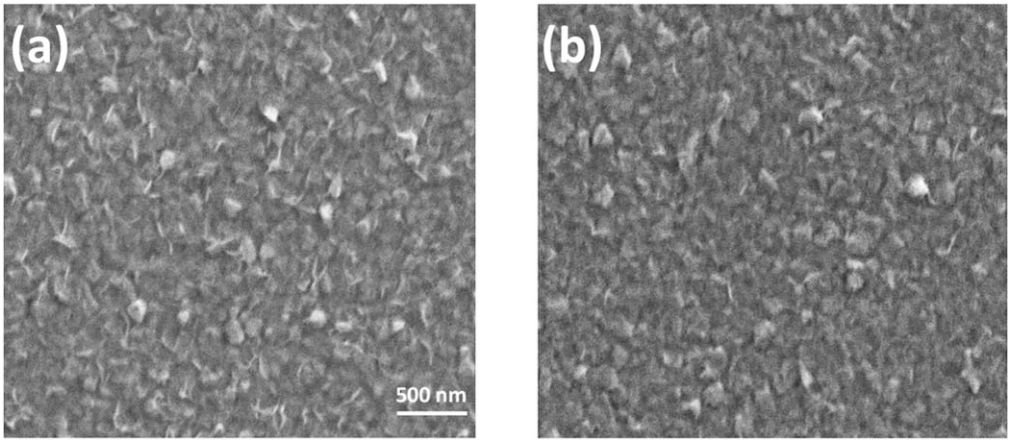

Figure 6. SEM images of cobalt nuclei deposited thin Co seed blanket wafer from solution containing 0.01 M Co with (a) 100-ppm FD and—2 mA cm^{-2} (b) 100-ppm FD and—4 mA cm^{-2} for 500 s.

confirmed to enhance the side reaction rate, but also the initial Co deposition was found to follow the progressive nucleation behavior for almost all cases. Galvanostatic deposition along with electron microscopic characterization was carried out and the nucleus shape, nucleation density as well as the morphology of thick films were found highly dependent on the FD concentration and deposition current.

Acknowledgments

National Science Foundation is acknowledged for support through Grant CMMI-1662332. YH thanks the Graduate Council at University of Alabama for a fellowship support. Brett Baker-O'Neal at SUNY Polytech and Ahmed Shafaat at GlobalFoundries were acknowledged for providing the Co seed substrates for the studies. Central analytical facility at the University of Alabama is acknowledged for the access of equipment for characterization.

References

1. W. Steinhögl, G. Schindler, G. Steinlesberger, and M. Engelhardt, "Size-dependent resistivity of metallic wires in the mesoscopic range." *Phys. Rev. B*, **66**, 075414 (2002).
2. W. Wu, S. Brongersma, M. Van Hove, and K. Maex, "Influence of surface and grain-boundary scattering on the resistivity of copper in reduced dimensions." *Appl. Phys. Lett.*, **84**, 2838 (2004).
3. M. H. van der Veen, N. Heyler, O. V. Pedreira, I. Ciofi, S. Decoster, V. V. Gonzalez, N. Jourdan, H. Struyf, K. Croes, and C. Wilson, *Damascene Benchmark of Ru, Co and Cu in Scaled Dimensions*, p. 172 (2018), in IEEE International Interconnect Technology Conference (IITC), IEEE2018.
4. R. L. Graham, G. Alers, T. Mountsier, N. Shamma, S. Dhuey, S. Cabrini, R. H. Geiss, D. T. Read, and S. Peddeti, "Resistivity dominated by surface scattering in sub-50 nm Cu wires." *Appl. Phys. Lett.*, **96**, 042116 (2010).
5. P.-I. Wang, M. D. Frey, M. Washington, S. Nayak, and T.-M. Lu, "Resistivity of sub-50 nm copper lines epitaxially grown on Si (100) substrate." *Thin Solid Films*, **520**, 6106 (2012).
6. M. He, X. Zhang, T. Nogami, X. Lin, J. Kelly, H. Kim, T. Spooner, D. Edelstein, and L. Zhao, "Mechanism of Co liner as enhancement layer for Cu interconnect gap-fill." *J. Electrochem. Soc.*, **160**, D3040 (2013).
7. C.-C. Wei, E. Chou, S. Shih, and S.-M. Lin, "Bottom-up filling of damascene trenches with cobalt by electroplating ;process." *228th Electrochemical Society Meeting Abstract, Phoenix, AZ, 2015* (The Electrochemical Society) p. 949 (2015).
8. M. Hayase, M. Taketani, K. Aizawa, T. Hatsuzawa, and K. Hayabusa, "Copper bottom-up deposition by breakdown of PEG-Cl inhibition." *Electrochem. Solid-State Lett.*, **5**, C98 (2002).
9. T. Moffat, D. Wheeler, W. Huber, and D. Josell, "Superconformal electrodeposition of copper." *Electrochem. Solid-State Lett.*, **4**, C26 (2001).
10. T. P. Moffat, J. Bonevich, W. Huber, A. Stanishevsky, D. Kelly, G. Stafford, and D. Josell, "Superconformal electrodeposition of copper in 500–90 nm features." *J. Electrochem. Soc.*, **147**, 4524 (2000).
11. T. P. Moffat, D. Wheeler, M. D. Edelstein, and D. Josell, "Superconformal film growth: mechanism and quantification." *IBM J. Res. Dev.*, **49**, 19 (2005).
12. S. H. Cha, S.-S. Kim, S. K. Cho, and J. J. Kim, "Copper bottom-up filling by electroplating without any additives on patterned wafer." *Electrochem. Solid-State Lett.*, **10**, D22 (2007).
13. C. H. Lee, S. C. Lee, and J. J. Kim, "Bottom-up filling in Cu electroless deposition using bis-(3-sulfopropyl)-disulfide (SPS)." *Electrochim. Acta*, **50**, 3563 (2005).
14. C. Chang, X. Lu, Z. Lei, Z. Wang, and C. Zhao, "2-Mercaptopyridine as a new leveler for bottom-up filling of micro-vias in copper electroplating." *Electrochim. Acta*, **208**, 33 (2016).
15. X. Lu, L. Yao, S. Ren, and Z. Wang, "A study of bottom-up electroplated copper filling by the potential difference between two rotating speeds of a working electrode." *J. Electroanal. Chem.*, **712**, 25 (2014).
16. P. Broekmann, A. Fluegel, C. Emnet, M. Arnold, C. Roeger-Goepfert, A. Wagner, N. Hai, and D. Mayer, "Classification of suppressor additives based on synergistic and antagonistic ensemble effects." *Electrochim. Acta*, **56**, 4724 (2011).
17. J. J. Kelly and A. C. West, "Copper deposition in the presence of polyethylene glycol I. Quartz crystal microbalance study." *J. Electrochem. Soc.*, **145**, 3472 (1998).
18. J. J. Kelly and A. C. West, "Copper deposition in the presence of polyethylene glycol II. Electrochemical impedance spectroscopy." *J. Electrochem. Soc.*, **145**, 3477 (1998).
19. J. Reid, "Copper electrodeposition: principles and recent progress." *Japan. J. Appl. Phys.*, **40**, 2650 (2001).
20. D. Josell and T. Moffat, "Extreme bottom-up filling of through silicon vias and damascene trenches with gold in a sulfite electrolyte." *J. Electrochem. Soc.*, **160**, D3035 (2013).
21. D. Josell, C. Beauchamp, D. Kelley, C. Witt, and T. Moffat, "Gold superfill in sub-micrometer trenches." *Electrochem. Solid-State Lett.*, **8**, C54 (2005).
22. D. Josell, D. Wheeler, and T. P. Moffat, "Gold superfill in submicrometer trenches: Experiment and prediction." *J. Electrochem. Soc.*, **153**, C11 (2006).
23. B. Baker, M. Freeman, B. Melnick, D. Wheeler, D. Josell, and T. P. Moffat, "Superconformal electrodeposition of silver from a KAg (CN) 2 KCN KSeCN electrolyte." *J. Electrochem. Soc.*, **150**, C61 (2003).
24. T. P. Moffat, B. Baker, D. Wheeler, J. E. Bonevich, M. Edelstein, D. Kelly, L. Gan, G. R. Stafford, P. Chen, and W. Egelhoff, "Superconformal electrodeposition of silver in submicrometer features." *J. Electrochem. Soc.*, **149**, C423 (2002).
25. B. Baker, C. Witt, D. Wheeler, D. Josell, and T. P. Moffat, "Superconformal silver deposition using KSeCN derivatized substrates." *Electrochem. Solid-State Lett.*, **6**, C67 (2003).
26. D. Josell, B. Baker, C. Witt, D. Wheeler, and T. P. Moffat, "Via filling by electrodeposition superconformal silver and copper and conformal nickel." *J. Electrochem. Soc.*, **149**, C637 (2002).
27. D. Josell, M. Silva, and T. P. Moffat, "Superconformal bottom-up Cobalt deposition in high aspect ratio through silicon vias." *J. Electrochem. Soc.*, **163**, D809 (2016).
28. M. A. Rigsby, L. J. Brogan, N. V. Doubina, Y. Liu, E. C. Opocensky, T. A. Spurlin, J. Zhou, and J. D. Reid, "Superconformal Cobalt fill through the use of sacrificial oxidants." *ECS Trans.*, **80**, 767 (2017).
29. M. A. Rigsby, L. J. Brogan, N. V. Doubina, Y. Liu, E. C. Opocensky, T. A. Spurlin, J. Zhou, and J. D. Reid, "The critical role of pH gradient formation in driving superconformal cobalt deposition." *J. Electrochem. Soc.*, **166**, D3167 (2019).
30. J. Wu, F. Wafula, S. Branagan, H. Suzuki, and J. van Eisden, "Mechanism of Cobalt bottom-up filling for advanced node interconnect metallization." *J. Electrochem. Soc.*, **166**, D3136 (2019).
31. M. Quinet, F. Lallemand, L. Ricq, J. Y. Hihn, P. Delobelle, C. Arnould, and Z. Mekhalif, "Influence of organic additives on the initial stages of copper electrodeposition on polycrystalline platinum." *Electrochim. Acta*, **54**, 1529 (2009).
32. D. Liang, J. Liu, K. Reuter, B. Baker-O'Neal, and Q. Huang, "Electroplating of Fe-Rich NiFe alloys in Sub-50 nm lines." *J. Electrochem. Soc.*, **161**, D301 (2014).
33. C. H. Lee, J. E. Bonevich, J. E. Davies, and T. P. Moffat, "Superconformal electrodeposition of Co and Co–Fe alloys using 2-Mercapto-5-benzimidazolesulfonic acid." *J. Electrochem. Soc.*, **156**, D301 (2009).
34. X. Zheng, Y.-N. Shi, and K. Lu, "The combination addition of 2-Mercapto-5-benzimidazolesulfonic acid and Thiourea to watts bath in controllable electro-healing cracks in nickel." *J. Electrochem. Soc.*, **163**, D349 (2016).
35. Y. Hu and Q. Huang, "Effects of dimethylglyoxime and cyclohexane dioxime on the electrochemical nucleation and growth of cobalt." *J. Electrochem. Soc.*, **166**, D3175 (2019).
36. Q. Huang, T. Lyons, and W. Sides, "Electrodeposition of cobalt for interconnect application: effect of dimethylglyoxime." *J. Electrochem. Soc.*, **163**, D715 (2016).
37. T. Lyons and Q. Huang, "Effects of cyclohexane-monoxime and dioxime on the electrodeposition of cobalt." *Electrochim. Acta*, **245**, 309 (2017).
38. F. G. Cottrell, "Der Reststrom bei galvanischer Polarisation, betrachtet als ein Diffusionsproblem." *Z. Phys. Chem.*, **42**, 385 (1903).
39. P.-A. Jacques, V. Artero, J. Pécaut, and M. Fontecave, "Cobalt and nickel diimine-dioxime complexes as molecular electrocatalysts for hydrogen evolution with low overvoltages." *Proc. Natl Acad. Sci.*, **106**, 20627 (2009).
40. F. Ma, D. Jagner, and L. Renman, "Mechanism for the electrochemical stripping reduction of the nickel and cobalt dimethylglyoxime complexes." *Anal. Chem.*, **69**, 1782 (1997).
41. C. N. Valdez, J. L. Dempsey, B. S. Brunschwig, J. R. Winkler, and H. B. Gray, "Catalytic hydrogen evolution from a covalently linked dicobaloxime." *Proc. Natl Acad. Sci.*, **109**, 15589 (2012).
42. C. C. McCrory, C. Uyeda, and J. C. Peters, "Electrocatalytic hydrogen evolution in acidic water with molecular cobalt tetraazamacrocycles." *JACS*, **134**, 3164 (2012).
43. N. Kaeffer, A. Morozan, J. Fize, E. Martinez, L. Guetaz, and V. Artero, "The dark side of molecular catalysis: diimine–dioxime cobalt complexes are not the actual hydrogen evolution electrocatalyst in acidic aqueous solutions." *ACS Catal.*, **6**, 3727 (2016).
44. N. Kaeffer, M. Chavarot-Kerlidou, and V. Artero, "Hydrogen evolution catalyzed by cobalt diimine–dioxime complexes." *Acc. Chem. Res.*, **48**, 1286 (2015).
45. K. Oura, V. Lifshits, A. Saranin, A. Zotov, and M. Katayama, in *Surface Science: An Introduction* (Springer Science & Business Media, Berlin) (2003).
46. G. Gunawardena, G. Hills, I. Montenegro, and B. Scharifker, "Electrochemical nucleation: part I. general considerations." *J. Electroanal. Chem. Interfac. Electrochem.*, **138**, 225 (1982).
47. B. Scharifker and J. Mostany, "Three-dimensional nucleation with diffusion controlled growth: Part I. Number density of active sites and nucleation rates per site." *J. Electroanal. Chem. Interfac. Electrochem.*, **177**, 13 (1984).
48. J. Mostany, J. Mozota, and B. Scharifker, "Three-dimensional nucleation with diffusion controlled growth: Part II. The nucleation of lead on vitreous carbon." *J. Electroanal. Chem. Interfac. Electrochem.*, **177**, 25 (1984).
49. M. Palomar-Pardavé, B. Scharifker, E. Arce, and M. Romero-Romo, "Nucleation and diffusion-controlled growth of electroactive centers: reduction of protons during cobalt electrodeposition." *Electrochim. Acta*, **50**, 4736 (2005).
50. J. Aldana-González, M. Romero-Romo, J. Robles-Peralta, P. Morales-Gil, E. Palacios-González, M. Ramírez-Silva, J. Mostany, and M. Palomar-Pardavé, "On the electrochemical formation of nickel nanoparticles onto glassy carbon from a deep eutectic solvent." *Electrochim. Acta*, **276**, 417 (2018).
51. L. H. Mendoza-Huizar, J. Robles, and M. Palomar-Pardavé, "Nucleation and growth of cobalt onto different substrates: Part I. Underpotential deposition onto a gold electrode." *J. Electroanal. Chem.*, **521**, 95 (2002).
52. L. H. Mendoza-Huizar, J. Robles, and M. Palomar-Pardavé, "Nucleation and growth of cobalt onto different substrates: Part II. The upd-opd transition onto a gold electrode." *J. Electroanal. Chem.*, **545**, 39 (2003).

53. I. Mejía-Caballero, J. Aldana-González, T. Le Manh, M. Romero-Romo, E. Arce-Estrada, I. Campos-Silva, M. Ramírez-Silva, and M. Palomar-Pardavé, "Mechanism and kinetics of chromium electrochemical nucleation and growth from a choline chloride/ethylene glycol deep eutectic solvent." *J. Electrochem. Soc.*, **165**, D393 (2018).
54. L. Heerman and A. Tarallo, "Theory of the chronoamperometric transient for electrochemical nucleation with diffusion-controlled growth." *J. Electroanal. Chem.*, **470**, 70 (1999).
55. A. Bhattacharjee, E. S. Andreiadis, M. Chavarot-Kerlidou, M. Fontecave, M. J. Field, and V. Artero, "A computational study of the mechanism of hydrogen evolution by cobalt (diimine-dioxime) catalysts." *Chem.—Eur. J.*, **19**, 15166 (2013).
56. G. Oskam and P. C. Searson, "Electrochemistry of gold deposition on n-Si (100)." *J. Electrochem. Soc.*, **147**, 2199 (2000).
57. A. Munoz, D. Salinas, and J. Bessone, "First stages of Ni deposition onto vitreous carbon from sulfate solutions." *Thin Solid Films*, **429**, 119 (2003).
58. C. Wang, Y. Wang, Y. Cheng, W. Huang, B. Zou, and X. Cao, "Effects of surfactants on the structure and crystal growth behavior of $Sm_2Zr_2O_7$ nanocrystalline." *Powder Technol.*, **225**, 130 (2012).
59. D. Kandel and E. Kaxiras, "Surfactant mediated crystal growth of semiconductors." *Phys. Rev. Lett.*, **75**, 2742 (1995).
60. L. I. Mosquera-Giraldo, N. S. Trasi, and L. S. Taylor, "Impact of surfactants on the crystal growth of amorphous celecoxib." *Int. J. Pharm.*, **461**, 251 (2014).